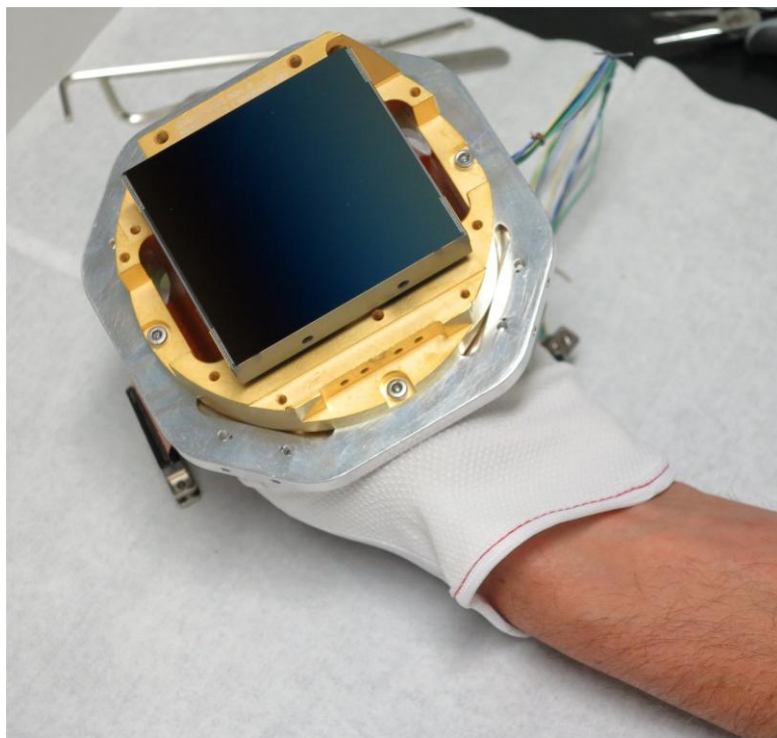


## Engineering Services for CCD System

### Final Report (Phase 3 Contract)

### Science CCD performance report

July 01<sup>st</sup> 2014



Simon Tulloch

FRACTAL

## 1. SUMMARY

This document describes the characterisation work done on the CARMENES science grade detector (serial number 08354-09-01). The CCD was optimised and characterised in the ESO head at the LICA laboratory. Cooling was done by a closed cycle cooler. The CCD was used in quad-readout mode and using differential video transmission with 300 Ohm resistors providing the -ve video signals. The use of quad readout meant that many parameters had to be measured four times. To present the data in a compact form many graphs show data from all four amplifiers plotted together using different colours for each one. The convention used is as follows: Amplifier G= red, Amplifier H= green, Amplifier E=blue and Amplifier F=yellow.

## 2. IMAGE DIMENSIONS

The image measures 4250 x 4200 pixels. Although read-out through four amplifiers the ARC software produces a single fits file which appears on the “ds9” image display tool as shown below in Figure 1. Also shown are the positions of the three mounting screws on the rear face of the CCD. The image displayed on DS9 is what one would see looking in through the front of the ESO cryostat when rotated so that the CCD connector is on the right.

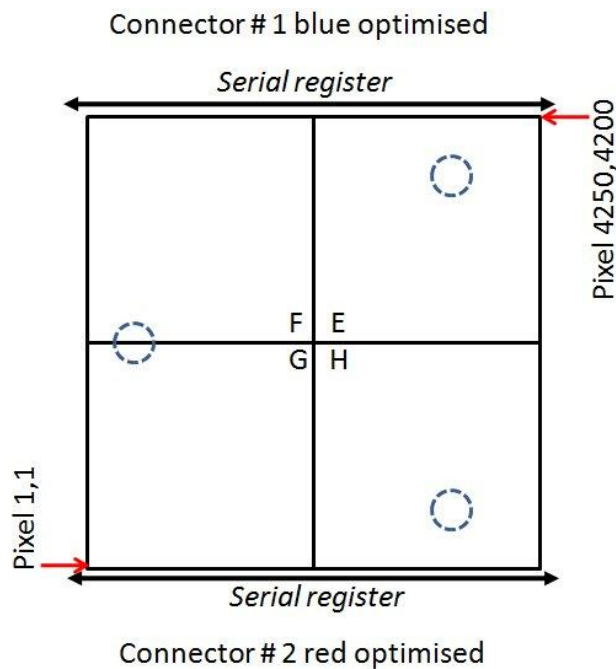


**Figure 1:** Image orientation and size

### 3. USE OF ESO HEAD WITH CLOSED CYCLE COOLER

No continuous flow cryostat was available so the science CCD was cooled using a Brooks polycold Cryotiger closed-cycle cooler. The arrangement is shown in Figure 2. The minimum temperature achieved was 189K.

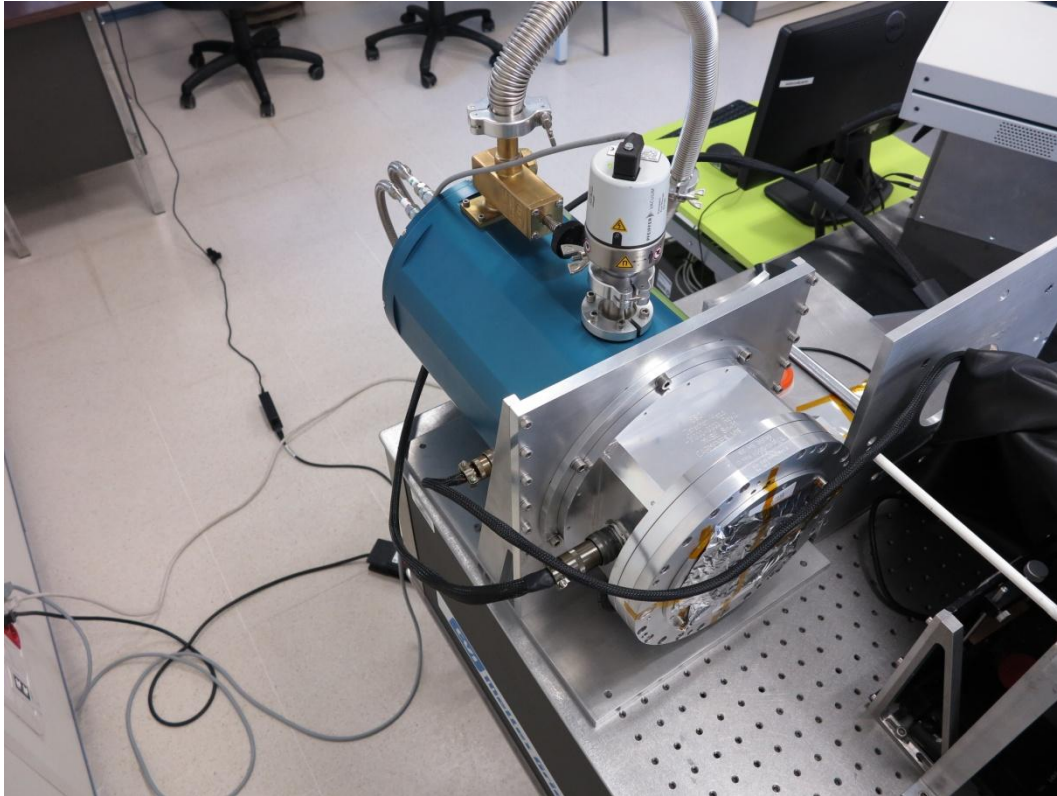


*Figure 2: ESO head coupled to a closed cycle cooler cryostat*

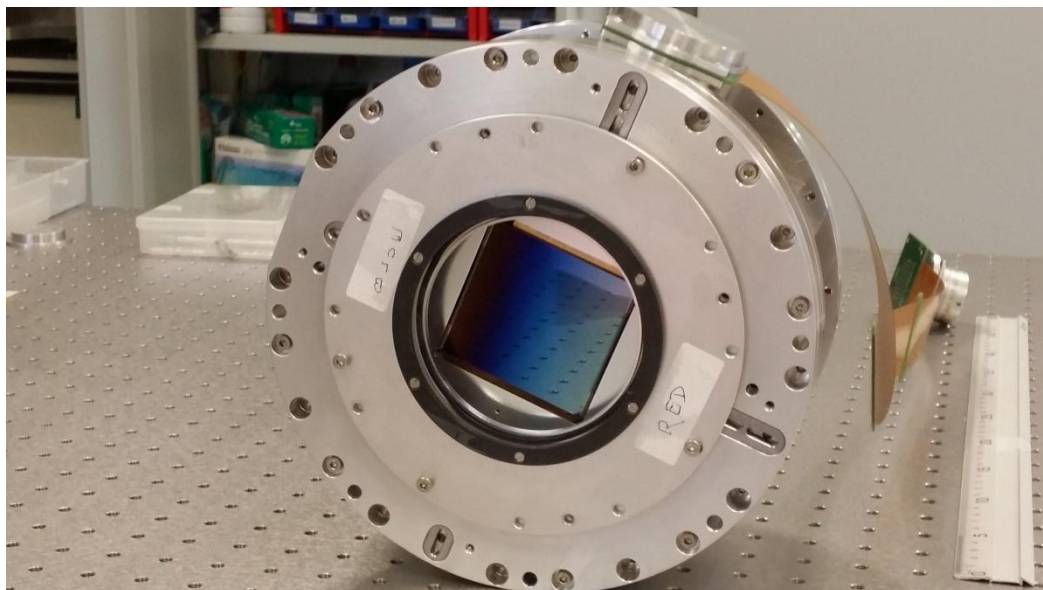


*Figure 3: ESO head with CCD mounted.*



#### 4. READOUT SPEEDS

Three readout speeds were implemented, Low speed (LSP), High Speed (HSP) and Engineering speed (ESP). The first two are intended for science, the third is strictly for engineering use as it is quite noisy. ESP has the advantage of including the full-well pixel signal within the ADC dynamic range. The performance of the three readout speeds is shown in Table 1. The inverse gain and noise is shown for each quadrant (ordered G, H, E, F). The noise was considerably improved by optimisation of the initial OD and RD voltage.

Speed	Readout time	Inverse gain (e/ADU) Amplifier order= G,H,E,F	Noise (e) Amplifier order= G,H,E,F	Pixel rate
LSP	30s	1.0, 0.96, 0.97, 1.0	3.3, 3.2, 3.3, 3.4	157kpix/s
HSP	21s	2.05, 1.97, 1.98, 2.05	4.3, 4.1, 4.2, 4.4	225 kpix/s
ESP	16s	4.4, 4.3, 4.2, 4.3	9.7, 8.7, 8.5, 9.9	301kpix/s

**Table1:** Readout speed performance characteristics

Slower read out speeds were experimented with to see if even lower noise could be achieved. This didn't give any advantage. For example slowing the readout to 47s gave 5e read noise and slowing to 75s also gave 5e noise. The 30s readout speed proved to be the optimum. The final LSP speed used CDS integration times of 1.96 $\mu$ s for the reference and 1.96 $\mu$ s for the signal with a 0.6 $\mu$ s gap between them. This CDS timing gives nulls at 385kHz, 500kHz, 769kHz and 1MHz i.e. the system is insensitive to interference at these frequencies (two of which are suspiciously round numbers).

The gains were calculated using the photon transfer technique. They were measured across a wide range of exposure levels. The general trend is for the gain to gradually rise with signal. This is a consequence of PSF loss at higher signal levels as pixels become "leaky" the fuller they become. This seems to have an onset at about 20ke-. The tabulated gain values used were taken from averages of the gain measurements at lower signal levels so as to avoid this effect.

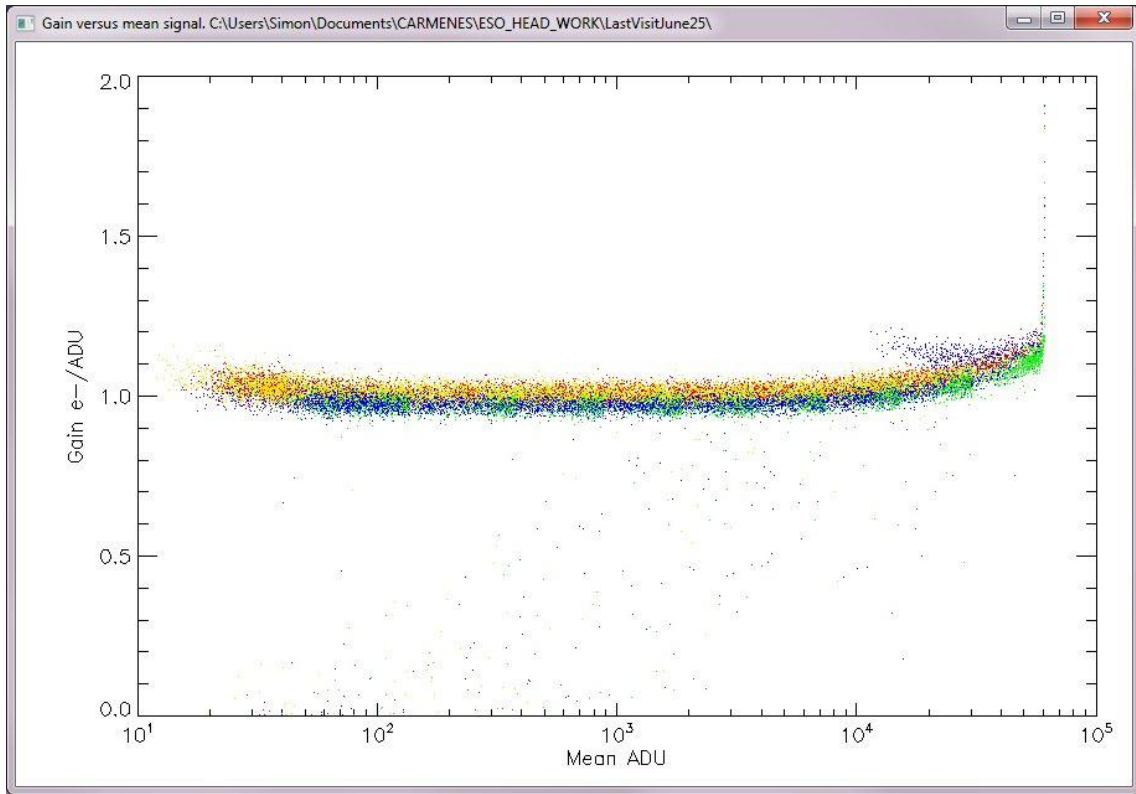


**Figure 4:** Photon transfer gain result for LSP

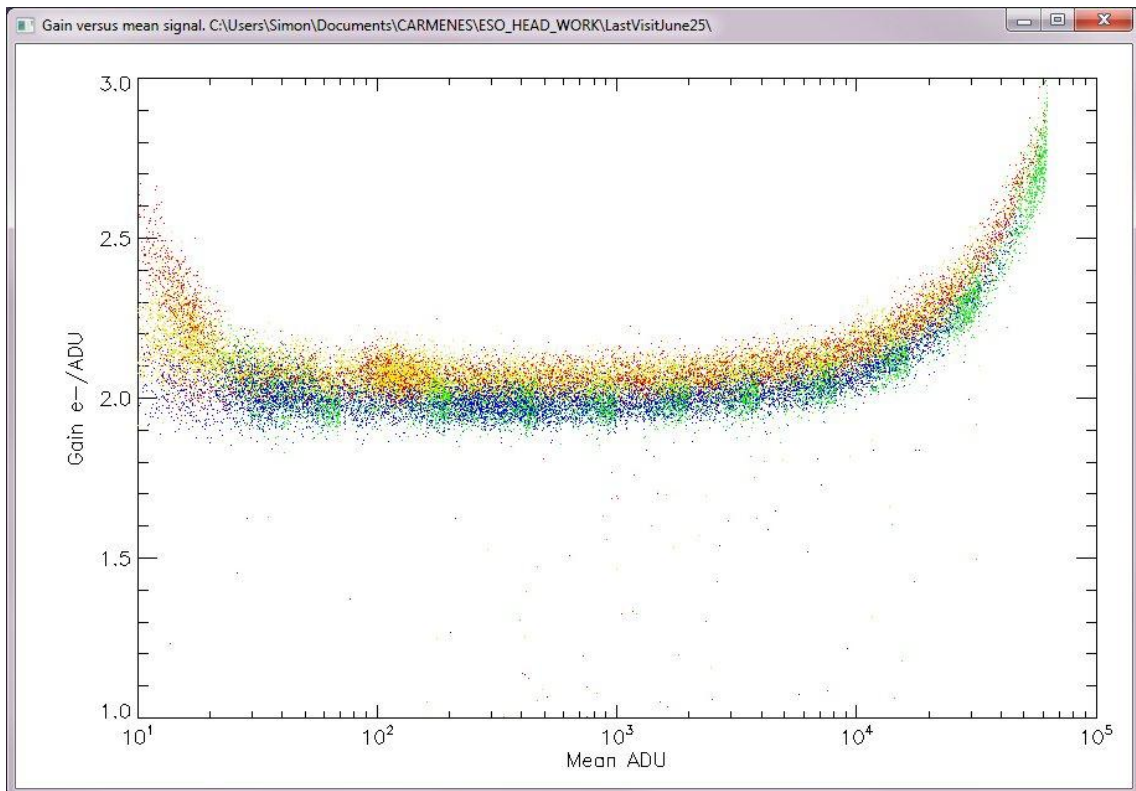


**Figure 5:** Photon transfer gain result for HSP

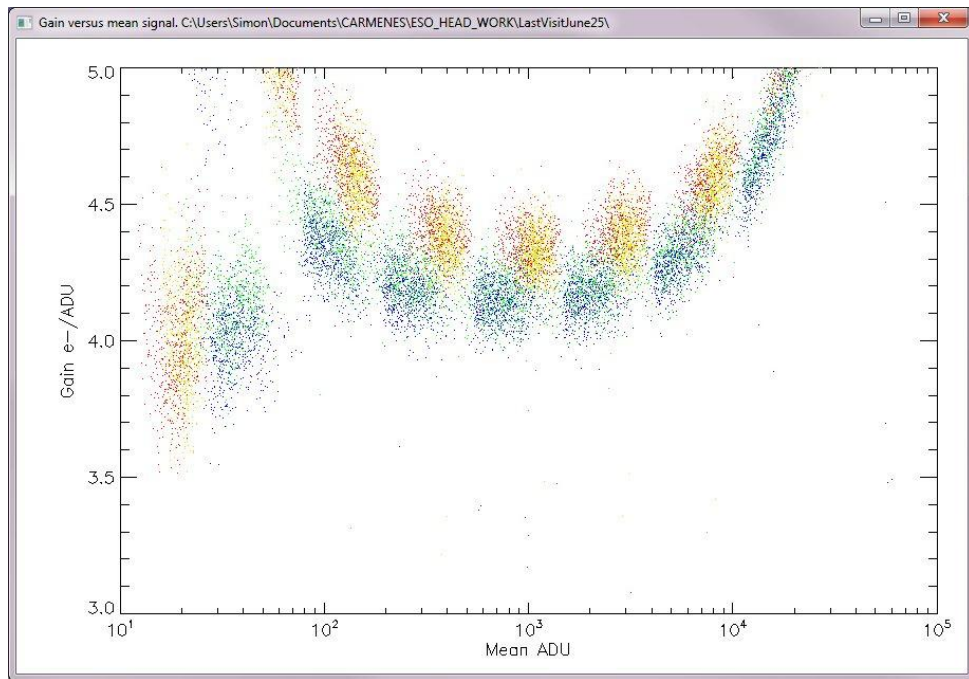


**Figure 6:** Photon transfer gain result for ESP

## 5. BIAS QUALITY

The bias frames were very clean and dominated by Gaussian noise. The differential video technique has been very effective at removing pattern noise.

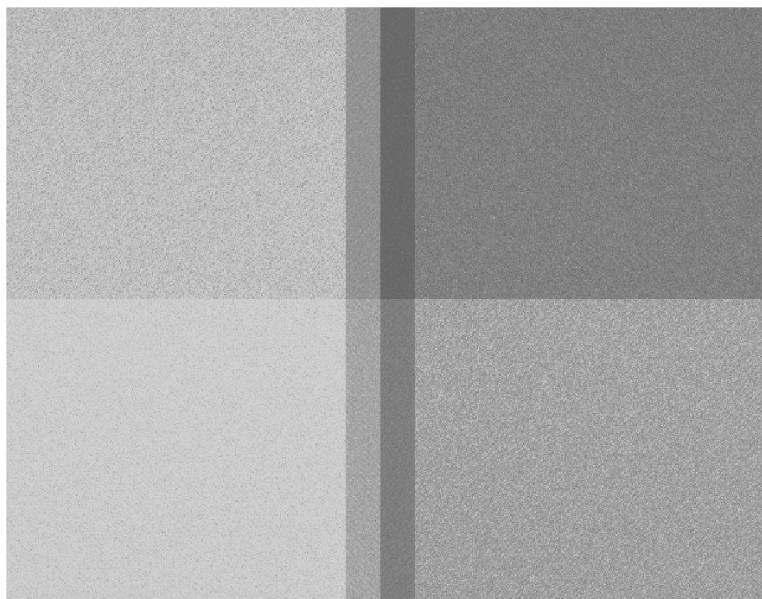


**Figure 7:** LSP bias frame showing centre of CCD. Some dark current accumulated during readout is visible.

## 6. LINEARITY

Linearity was measured using the internal cryostat pre-flash LED. The exposure time was gradually stepped up until the ADC saturation level was reached in LSP and HSP. A graph was made of exposure time versus mean signal in a small measurement box. A line fit was then made between the origin and the first data point with an exposure level above 3000 ADU. The error between the actual data points and the line fit was then plotted as a percentage error. The data is shown in Figures 8 and 9.

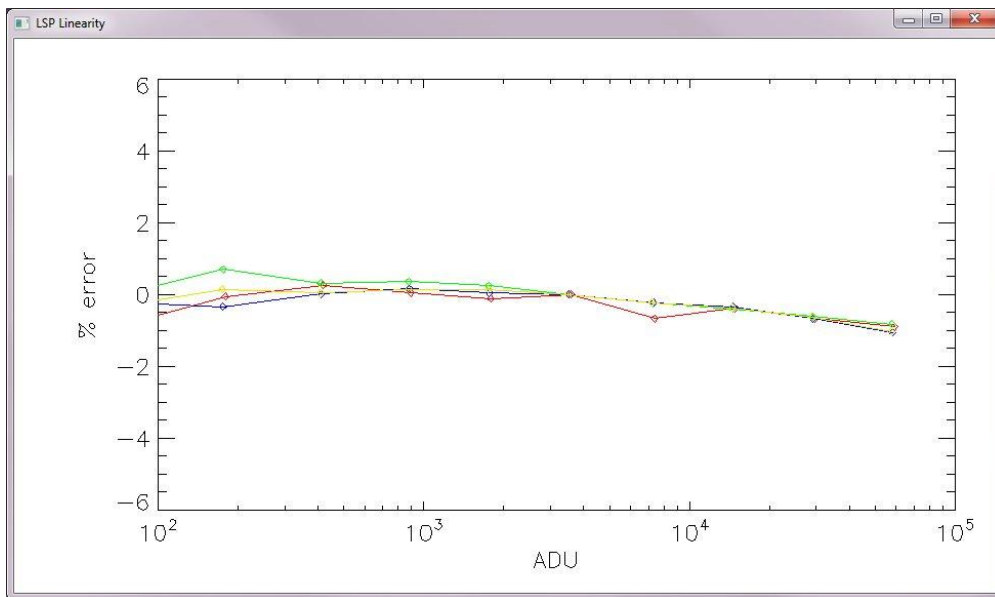


**Figure 8: LSP linearity errors**

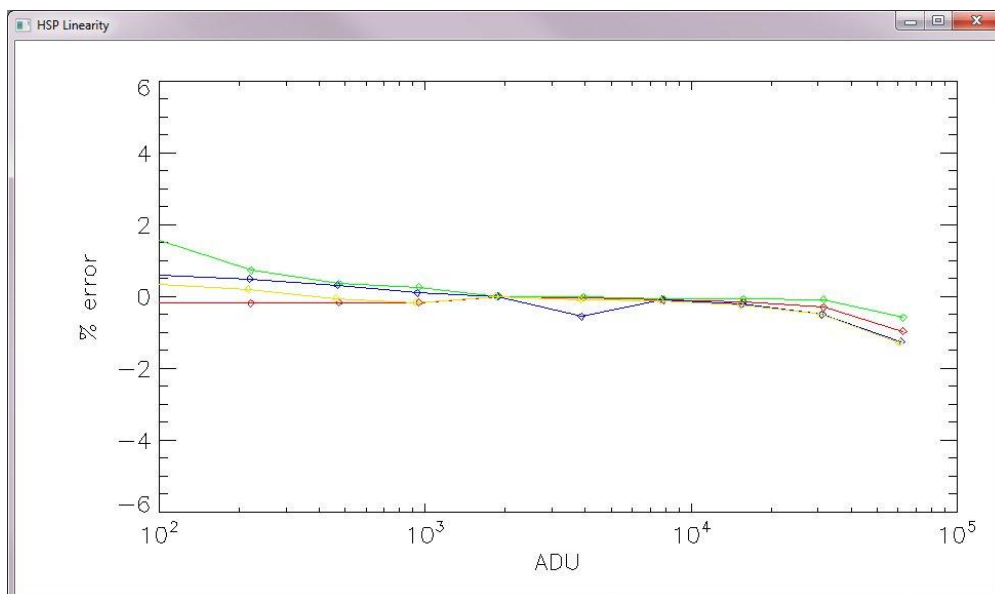


**Figure 9: HSP linearity errors**

## 7. FULL WELL

This was measured by incrementing the exposure level and observing how the variance in the signal increased with the mean. The full well exposure level is indicated by a sudden drop in variance. Mean versus variance was plotted in all three readout speeds. For Figures 10 and 11 the variance drop was due to ADC saturation. In Figure 12 it was due to the CCD reaching full well. Given that the ESP gain was measured at between 4.1 and 4.4e /ADU and the variance peaked at 60kADU we can calculate the full well as approximately 260ke-. The device-specific data sheet gave a value of 418ke- and it is not clear why we have not reached that value. The minimum specified value for this kind of CCD is 275ke-.

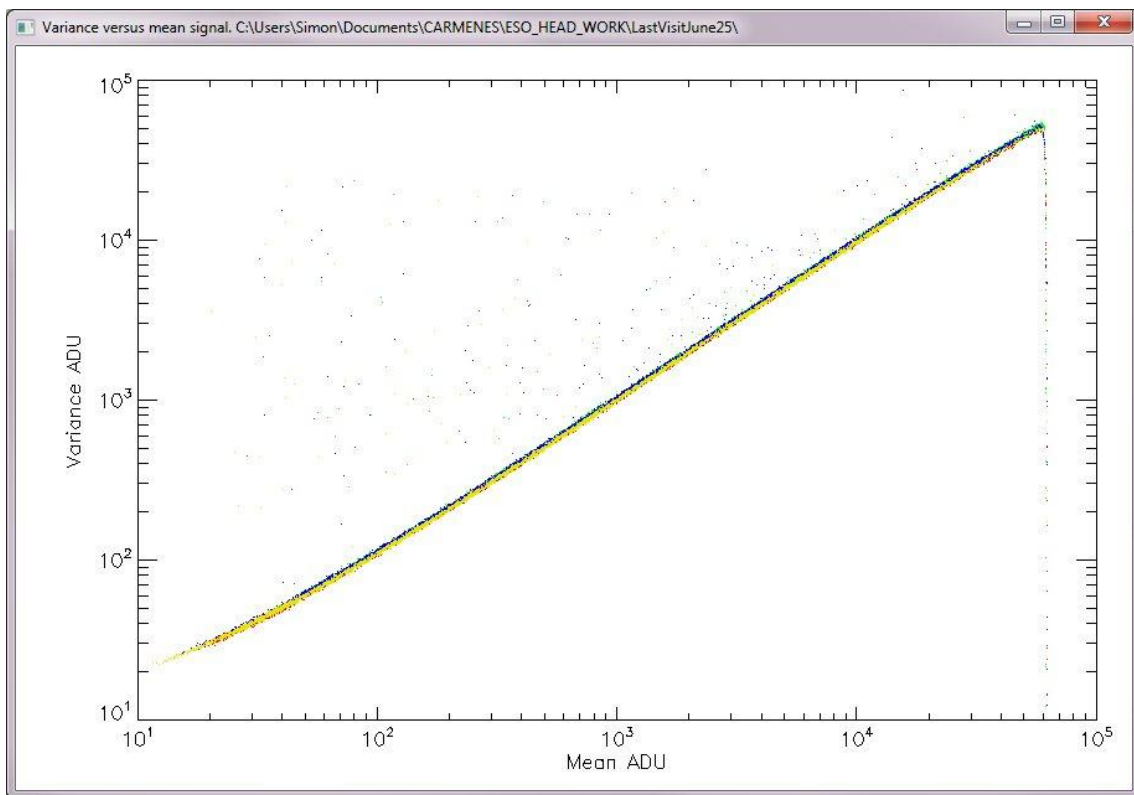


**Figure 10:** LSP Mean versus variance

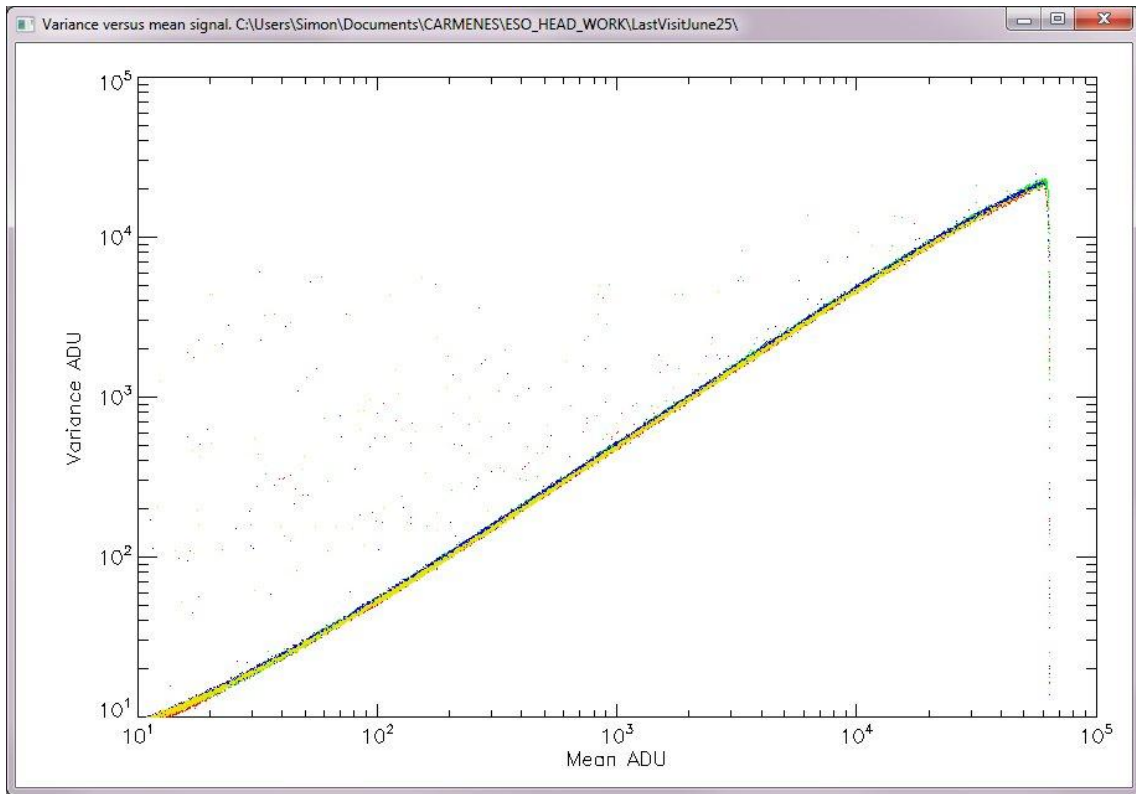


**Figure 11:** HSP Mean versus variance

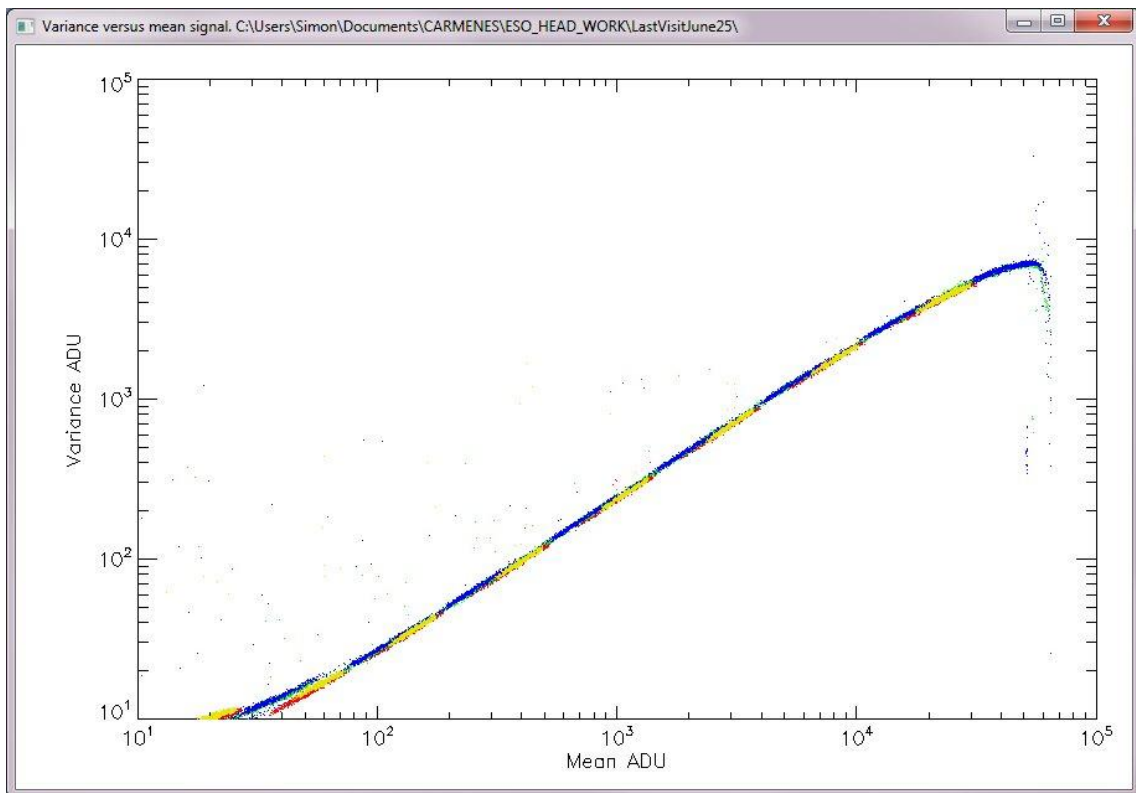


**Figure 12:** ESP Mean versus variance showing position of full well

## 8. DARK CURRENT

Unfortunately this was not measured. Dark frames were taken but later found to be contaminated with either stray light from the laboratory or from the internal preflash LED (in case that was inadvertently left on). Figure 13 shows the appearance of the dark frame showing the effects of light leaking in from the sides. The 2:1 variation between centre and edge rules out any thermal origin of this dark current since it would require about a 7K temperature differential across the chip. Thermal models from E2V show that the thick metal package equalises the temperature to less than a degree between centre and edge.

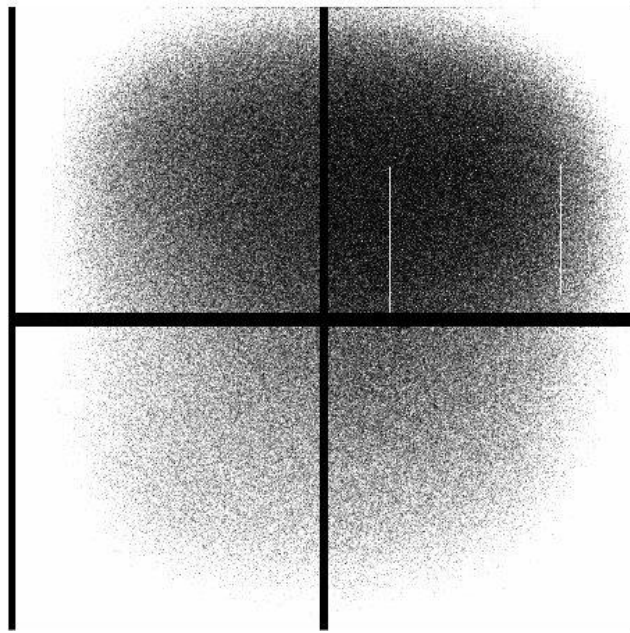


**Figure 13:** 600s dark frame at 189K. Contaminated by stray light.

## 9. COSMETICS

The CCD is a top grade science device so we should expect good cosmetics. Defective columns were visible were in quadrant E (top-right as displayed by ds9). A large cluster of defects was visible in a 10 x 40 pixel box centred on  $x=2561$ ,  $y=3118$ . This cluster produced two bright columns ( $x=2559$  and  $2565$ ) that extended over most of the quadrants height. A blocked permanently-black column was also located at  $x=3712$ . Some of the charge transferred down this column leaks into the neighbouring 2 columns when it transfers through the trap responsible (in row 3147) so in reality three columns are affected. The defect in column 3712 seems to leave some charge in the y-overscan of quadrant H i.e. not the quadrant of origin. It is not clear how this happens but it could be due to some bug in the Clear routine that needs to be further investigated.



**Figure 14:** Cluster of defects visible in quadrant E (centred on  $x=2561,y=3118$ )

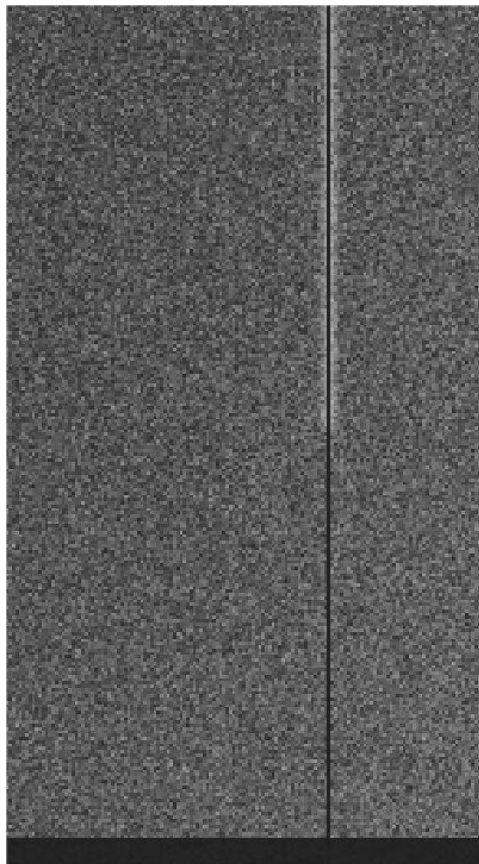


**Figure 15:** A blocked column visible in quadrant E (col 3712)

## 10. FRINGING

Illumination was done using an integrating sphere with a 20mm aperture placed 700mm from the CCD. Fringing was really excellent and only visible above the photon noise in a 950nm flat field. A fringed frame is shown in Figure 16. The top of this frame is the blue-optimised end, the bottom is red optimised. Note that the fringes are only visible in the blue optimised region i.e. the region where no red light should ever fall. This frame shows the effectiveness of a red-optimised AR coat in not only boosting red QE but also in suppressing fringing.

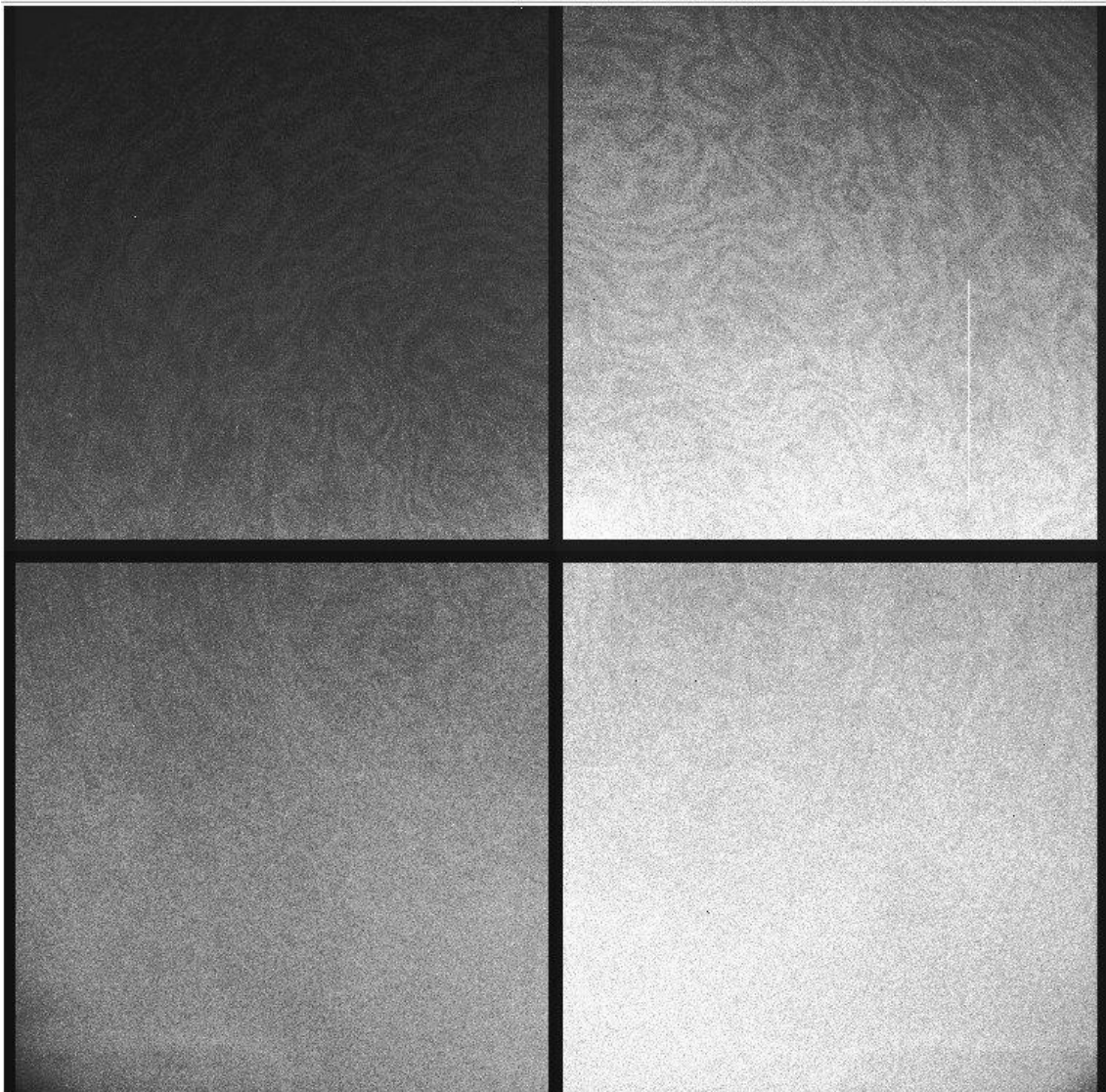


**Figure 16:** 950nm flat field

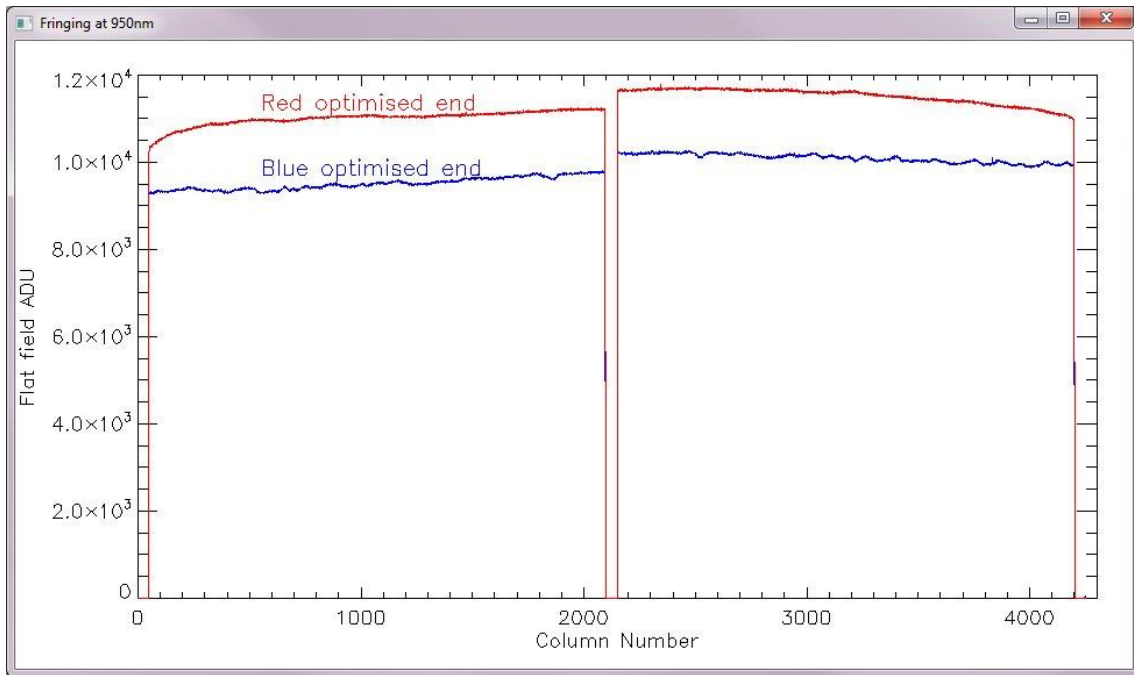


**Figure 17:** Horizontal cuts through 950nm flat field (Fig 16) showing fringing only in blue optimised end.

Figure 17 shows two horizontal cuts through the frame in Fig 16 at rows 100 and 3900. Fringing amplitudes of a few percent are visible at the blue end but at the red end there is nothing visible.

## 11. CROSSTALK

A bright spot just above full well was projected onto quadrant H. A cut was plotted through the spot maximum on both the illuminated quadrant and also through the corresponding image regions in the other three quadrants. The cuts were compared to see if there was any electronic crosstalk. Adjacent quadrants were found to contain ghosts of amplitude 0.02%. The diametrically opposed quadrant contained a ghost of 0.001% amplitude. Figure 18 shows the measurement frame. This is a magnified view of the centre of the frame where the 4 quadrants meet. There are also some optical ghosts visible.

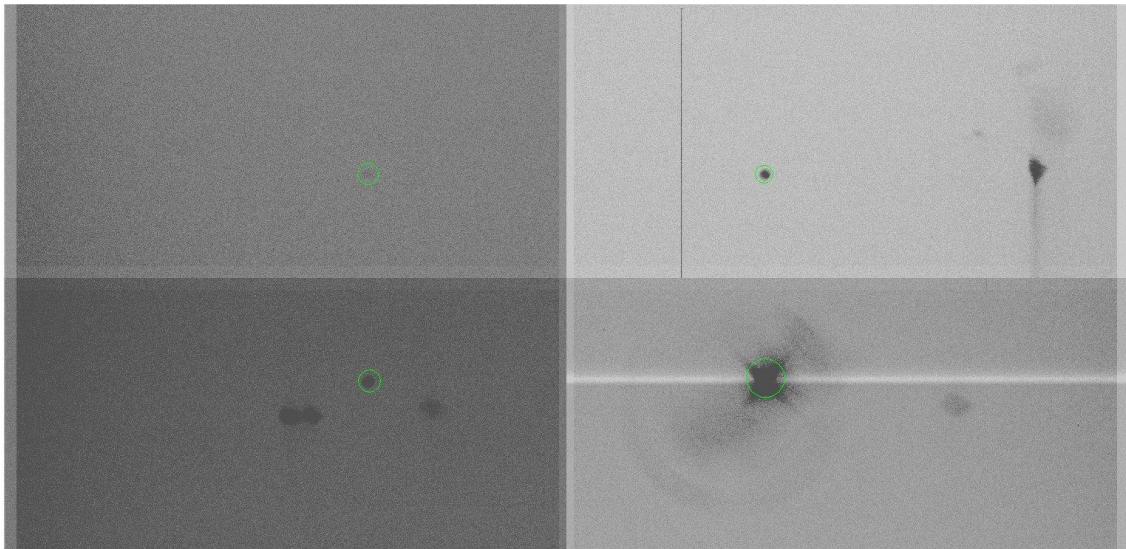


**Figure 18:** Crosstalk from an above-full well artificial star. Green circles show position of primary image (bottom right) and its three ghosts.

## 12. QUANTUM EFFICIENCY

This was measured in imaging mode using illumination from the integrating sphere. First the light intensity from the sphere was measured using a calibrated photodiode. The diode was then removed and the CCD located in the same plane as previously occupied by the diode. Flat fields were then taken. This method allowed the QE to be measured simultaneously across the whole CCD so as to see the effect of the graded AR coating.

This method of QE measurement is much less precise than the diode-mode method used in the test camera because it accumulates errors made in the measurement of the CCD gain, in the mechanical positioning of the diode and in the unevenness of the flat field. No allowance has been made for the window supplied by ESO whose transmission is unknown.

The data clearly shows the behaviour of the AR coating and confirms that the upper part of the chip is blue optimised and the lower part red optimised. Peak QEs are around 95%.

The measurements were taken at 189K. At temperatures of 160K (operational) the red QE will be considerably lower.

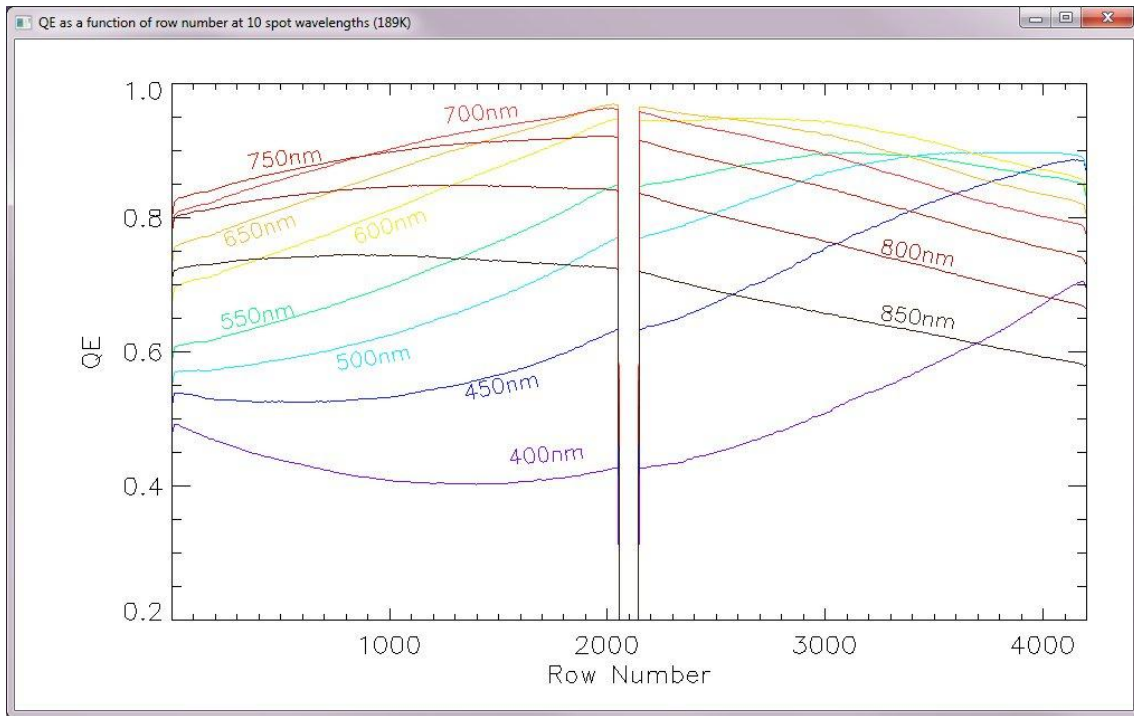


**Figure 19:** Quantum efficiency as a function of row number

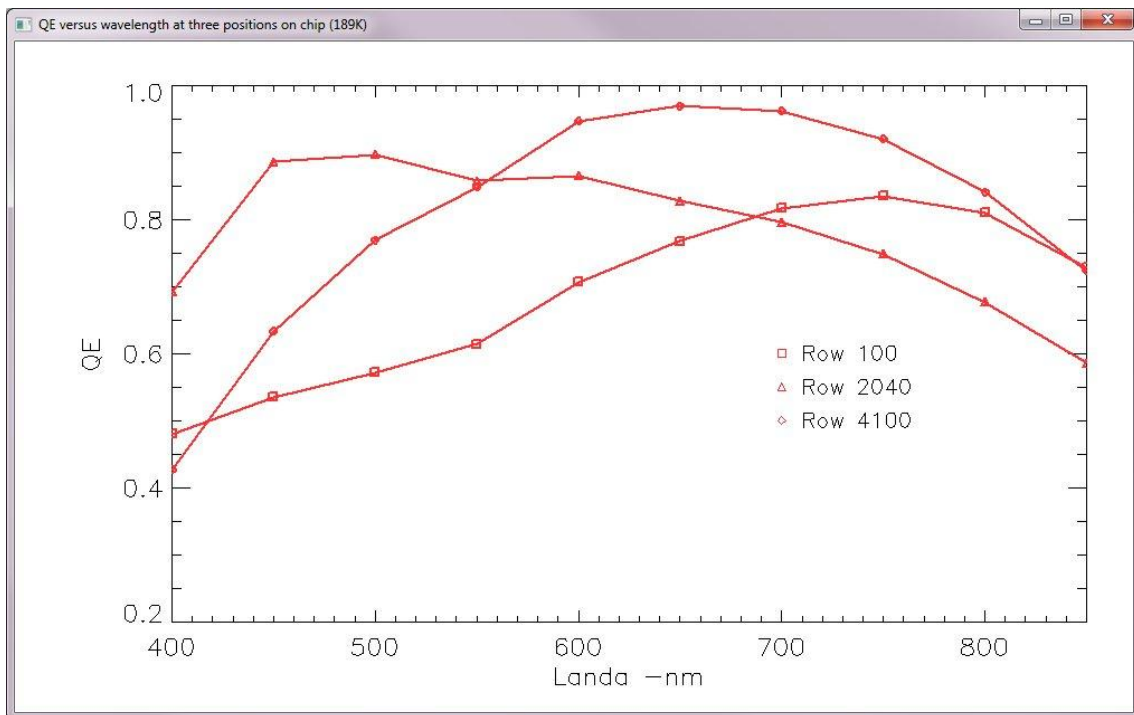


**Figure 20:** Quantum efficiency as a function of wavelength

### 13. POINT SPREAD FUNCTION

A 75mm focal length doublet was placed in front of the cryostat window and used to image a 25 $\mu$ m pinhole some 700mm distant. The pinhole was illuminated by a 450nm monochromator source. This produced an artificial star image on the CCD. The best focus was then found by fine adjustment. The experimental setup is shown in Figure 21.



*Figure 21: PSF measurement setup.*

Blue-end PSF is not quoted in the E2V data sheet and the concern is that these extra-thick deep depletion CCDs may suffer from blue-end PSF degradation due to charge diffusion. A surface plot of the artificial star image is shown in Figure 22. The central pixel contains 45% of the total signal showing that charge diffusion is not a problem.

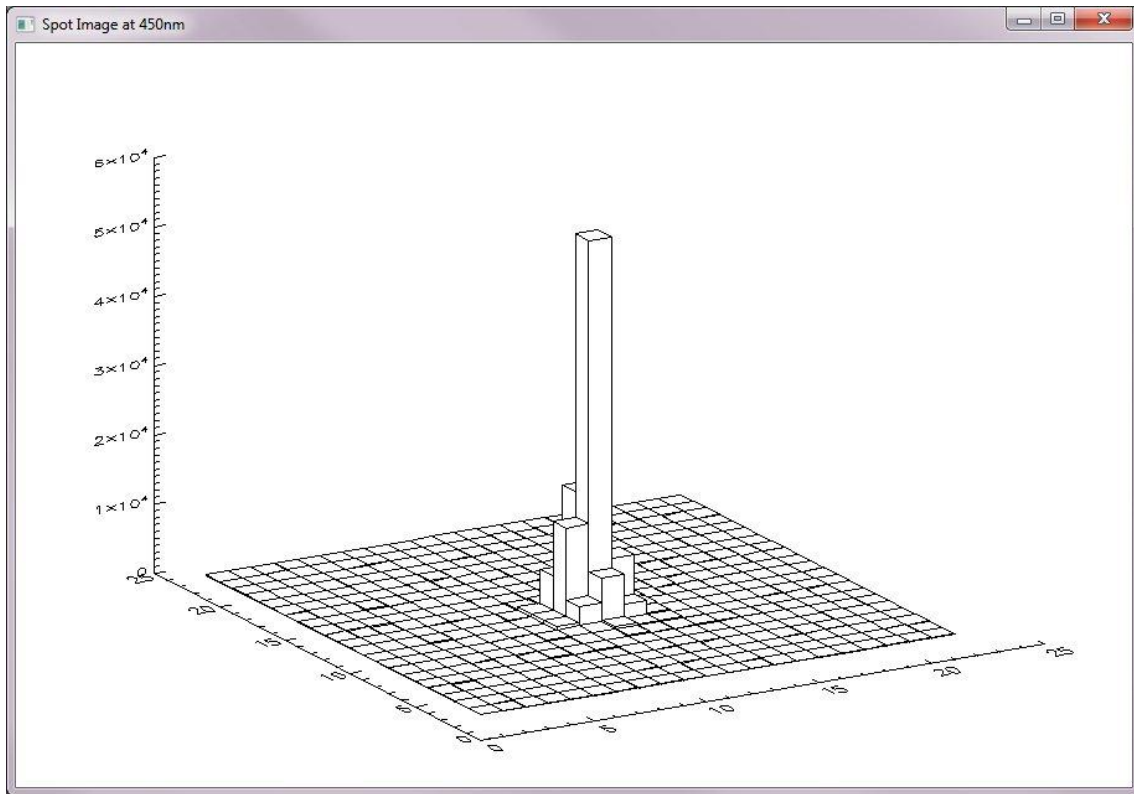


**Figure 22:** PSF measurement at 450nm

## 14. CHARGE TRANSFER EFFICIENCY

This was measured in both axes using the Extended Pixel Edge Response method. This involves measuring the amount of charge that is left behind in the first row of vertical overscan and the first column of horizontal overscan. It was important to mask out the faulty columns (those containing traps) when doing this calculation. It was also necessary to compensate for the slight vertical signal gradient produced by the dark current. Charge transfer efficiency was found to be excellent in the horizontal axis and essentially perfect in the vertical axis.

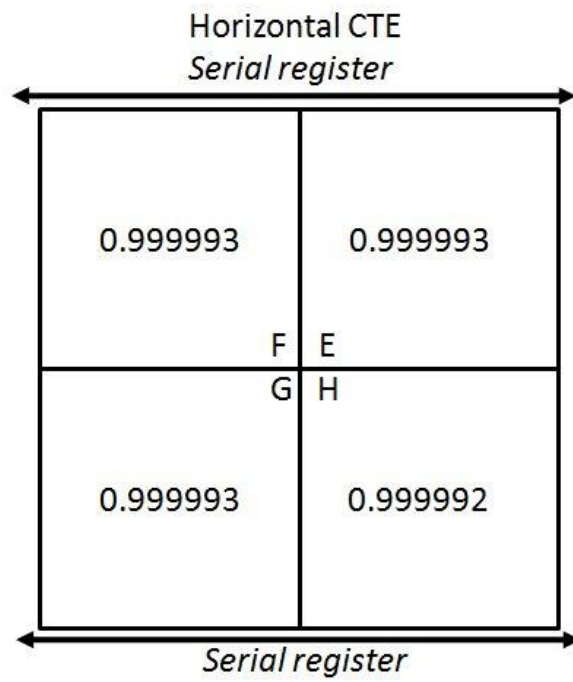


**Figure 23:** Horizontal Charge Transfer Efficiency

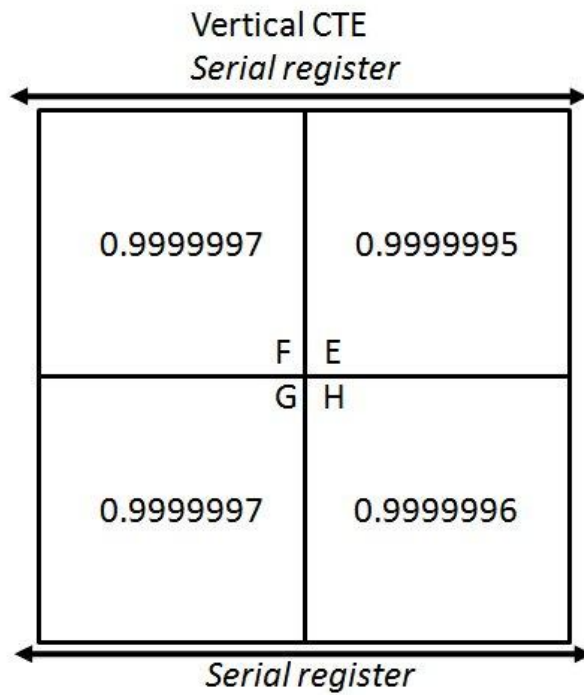


**Figure 24:** Vertical Charge Transfer Efficiency



## 15. NOTES ON CONTROLLER COMMANDS

The following new commands have been implemented on the controller. These are in addition to the standard ARC exposure and readout commands.

**LSP** select low speed

**HSP** select fast speed

**ESP** select engineering speed

**FLA n** flash the internal LED for n milliseconds prior to all following exposures (max 2200ms)

## 16. CONCLUSIONS

This is an excellent CCD especially well suited for red-end observations. The graded AR coat maximises the QE and minimises the fringing. The QE across the whole spectrum is state-of-the-art. The CCD is constructed using 50um thick deep-depletion silicon but this does not seem to adversely affect the PSF at 450nm. Cosmetically there are some problems but the CCD falls within specification. There is one dark column and four bright columns. The noise quoted on the data sheet at pixel rates of 50kHz (i.e. 90s readout time) reaches as low as  $2e^-$ . This was not reproducible since noise in the test system was found to rise at pixel rates below 160kHz. Minimum measured noise was  $3.2e^-$ . Full well was quite a bit lower than that quoted in the data sheet but  $260ke^-$  is still a high value and a factor of two above the ADC limit in the HSP readout speed. The dark current was not measured in the ESO head due to light leakage problems, however, the dark current of the engineering chip in the test cryostat was measured and found to agree with the E2V model so there is no reason to believe that the science chip should be any different. The data sheet dark current value is  $0.21e^-/pix/hour$  at 173K. A summary can be found in table 2.



Parameter	Measured	E2V data sheet
	Amplifier order= G,H,E,F	Amplifier order= G,H,E,F
Read noise e- (minimum)	3.3, 3.2, 3.3, 3.4	2.0,2.1,2.5,2.1
HCTE	0.999993,0.999992,0.999993, 0.999993	0.999995, 0.999997, 0.999997, 0.999997
VCTE	0.9999996	0.999996
Full Well	260ke-	418ke-
QE % 450nm	96	93
QE % 500nm	96	96
QE % 600nm	95	97
QE % 700nm	96	96
QE % 800nm	85	90
QE % 850nm	75	/
QE % 900nm	/	58
Bright columns	4	2
Dark columns	1	1

**Table2:** Comparison with E2V data sheet